

Hurricane formation in diabatic Ekman turbulence

David A. Schechter* and Timothy J. Dunkerton

NorthWest Research Associates, Redmond, WA, USA

ABSTRACT: This article investigates the emergence of hurricanes from chaotic swirling motions in a three-layer model of the tropical troposphere that includes basic parametrizations of cumulus convection and air–sea interaction. The chaotic flow is referred to as diabatic Ekman turbulence (DET), in order to emphasize that cumulus convection and Ekman pumping are critical to its behaviour. The time required for hurricane formation in DET is examined over a broad range of sea-surface temperatures, tropical latitudes and surface exchange coefficients for moist entropy and momentum. The mean trends are sensible, but for a given set of parameters, the genesis time can vary significantly with subtle changes to the initial turbulence. Moreover, hurricanes do not always form. In the event that a tropical depression develops into a hurricane, the process is highly asymmetric. Intensification involves a shear-flow instability, the production of mesovortices and contraction of the basic circulation. Despite the complex evolution, the intensification rate is largely consistent with the expectations of a quasi-linear stability analysis. Properties of mature hurricanes and the nature of their fluctuations are discussed in the context of the model. Copyright © 2009 Royal Meteorological Society

KEY WORDS tropical cyclones; turbulence; simple models

Received 25 May 2008; Revised 12 February 2009; Accepted 18 February 2009

1. Introduction

Today there exist remarkably intricate numerical models of the atmosphere designed for accurately predicting weather or climate. However, the complexity that is required for precise forecasting can obscure the fundamental mechanisms that govern atmospheric dynamics. In order to gain insight, it is common practice to use simpler models (Gill, 1982; Pedlosky, 1987; Holton, 1992). The optimal model depends on the problem at hand. This article is concerned with the emergence of hurricanes from chaotic swirling flows over tropical oceans, and how the process varies with sea-surface temperature (SST), latitude and surface exchange coefficients. Results are examined from a three-layer model of the troposphere that includes minimal parametrizations of cumulus convection and air–sea interaction. The parametrizations are based on the seminal hurricane model of Ooyama (1969) (O69; see also DeMaria and Schubert, 1984; DeMaria and Pickle, 1988; Shapiro, 1992, 2000; Dengler and Reeder, 1997; Arakawa, 2004).

Before presenting specifics of the three-layer model, let us briefly illustrate the process by which it creates hurricanes from random noise. It is helpful to describe this self-organization by comparison with a dry flow with no ambient rotation and no surface friction. Figure 1 shows that in both cases the early evolution is strongly influenced by two-dimensional (2D) cascade processes, such as vortex mergers and filamentation. Without convection or rotation, coalescence of like-sign vortices

would continue until the system becomes a synoptic-scale dipole. With convection (regulated by air–sea interaction) and rotation, a gradual cyclonic skew develops until the flow explosively transforms into a single dominant hurricane. The rapid transformation will be analyzed in a later section. The process of hurricane formation shown here is not merely the intensification of an isolated cyclone, but the creation of a distinguished vortex that is able to intensify while exposed to ambient shear and competition for moisture with its neighbours.[†]

Henceforth, we will use the term ‘diabatic Ekman turbulence (DET)’ to refer to chaotic flows from which hurricanes may emerge in a simple moist model that includes surface friction. DET is here viewed as a generalization of Ekman turbulence (ET), which refers to quasi-2D turbulence under the influence of surface friction alone. Whereas ET has received considerable attention in the fluid dynamics literature (Boffetta *et al.*, 2000; Nam *et al.*, 2000; Danilov and Gurarie, 2001; Celani *et al.*, 2004), DET is a relatively unexplored paradigm. In ET, surface friction tends to dissipate vortices. In DET, deep convection has the potential to counter Ekman spin-down and generate hurricanes (Smith, 2000). With this new terminology at hand, we may state our goal as follows: to elucidate hurricane formation in DET. The purpose of this article is to present the basic phenomenology of the process. Subsequent articles will examine more deeply the factors that promote or inhibit genesis.

While of interest in itself as a dynamical system, the relevance of DET to tropical dynamics depends on the

*Correspondence to: D. A. Schechter, NorthWest Research Associates, 4118 148th Ave NE, Redmond, WA 98052, USA.
E-mail: schechter@nwra.com

[†]See section 3.3 for further discussion of Figure 1.

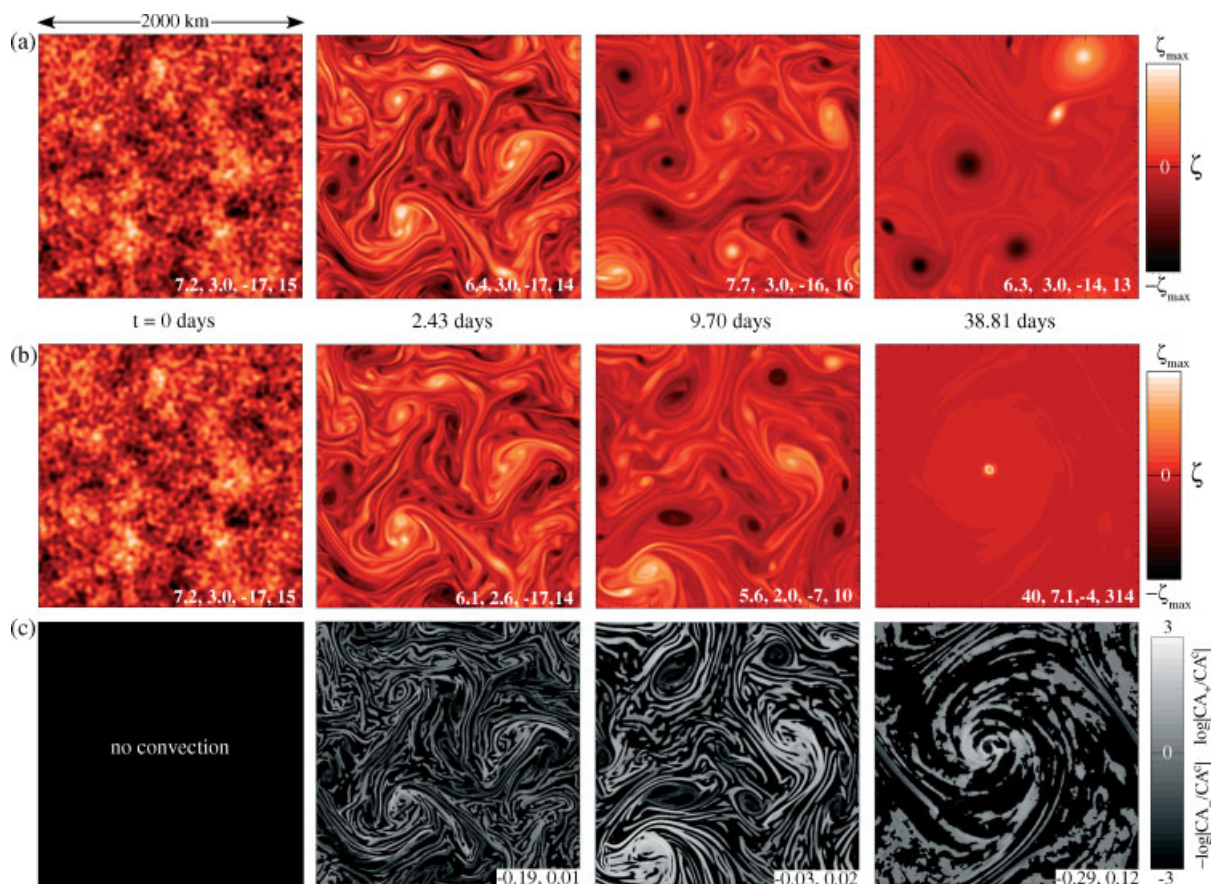


Figure 1. The self-organization of turbulence in two numerical experiments with a three-layer model of the troposphere on the periodic f -plane. (a) Evolution of relative vorticity ζ in the middle layer of a dry troposphere with no surface friction and no ambient rotation. (b) Same for a moist troposphere at 20°N , with active parametrizations of cumulus convection and surface friction; here the turbulence transforms into a hurricane. In both (a) and (b), the upper and lower limits of the colour scale are instantaneously adjusted to plus and minus the maximum of ζ . The lower right corner of each plot lists (from left to right) the following statistics of the middle layer: the maximum wind speed, the rms wind speed, the minimum ζ and the maximum ζ . The wind speeds and vorticities are in units of m s^{-1} and 10^{-5} s^{-1} , respectively. (c) Evolution of cumulus activity in the experiment with parametrized convection. Bright or dark shades represent regions of predominantly deep or shallow convection; the black area contains clear-air subsidence or no convection. See section 3.3 for the measure of cumulus activity (CA, Equation (25)) that was used to construct this figure. The numbers on the lower right corner of each plot give the instantaneous minimum and maximum values of CA in m s^{-1} . The hurricane images (at $t = 38.81$ days in (b) and (c)) are shifted relative to all others, such that the vortex is nearly at the centre.

specific model that is used for its study. There is little debate that the foundational hurricane model of Ooyama (O69) produces sensible variation of tropical cyclone intensity with the SST and the parameters of air–sea interaction. The O69 model predicts that the vortex intensifies with increasing values of the SST or the surface-exchange coefficient for moist entropy, but weakens with greater surface drag. These results are consistent with both cloud-resolving numerical simulations (Rotunno and Emanuel, 1987) and steady-state hurricane theory (Emanuel, 1986, 1995b). In further agreement with more complex models, those based on O69 can produce tropical cyclones in atmospheres that are initially stable to deep convection, due to a wind-induced surface flux of moist entropy (DeMaria and Pickle, 1988; Dengler and Reeder, 1997). Based on the qualified success of the O69 model in simulating isolated tropical cyclones, we believe that our generalized version should also provide useful insight into tropical cyclone development amid turbulence.

This is not to say that a three-layer model of such simplicity is perfect (Ooyama, 1982), or better than others.

Alternative parametrizations of convective processes may produce different pathways of hurricane formation in DET (Emanuel, 1989, 1995a; Raymond, 1995, 1997; Zehnder, 2001; Zhu *et al.*, 2001; Zhu and Smith, 2002; Arakawa, 2004). One essential reason is well-known: whereas O69-like models limit cumulus convection to regions of convergence in the boundary layer, others allow surface fluxes of moist entropy to initiate cumulus activity in regions of zero or negative convergence. In our view, this limitation does not severely diminish the ability of an O69-like model to capture the basic effects of nearby vortices and filaments on the growth and behaviour of a convective cyclone. The study of DET is intended to shed light on just these effects, as opposed to all aspects of hurricane formation and dynamics.

A more specific concern relates to the role of surface friction. Cloud-resolving numerical simulations have shown that surface friction is unnecessary for the transformation of a tropical depression into a hurricane (Craig and Gray, 1996). On the other hand, models based on O69 seem to require Ekman pumping to sustain intensification.

Such models therefore become inconsistent with their cloud-resolving counterparts as surface friction tends to zero. This discrepancy does not seem to be a critical deficiency for most purposes, since realistic values of the surface drag coefficient are known to produce realistic cyclone intensification rates. For the purpose of investigating how variation of surface drag affects the rate of hurricane formation in turbulence, using the O69 paradigm is more questionable. Nevertheless, the results of such a study are presented in order to describe fully the behaviour of our model.

To conclude the Introduction, we note that the study of moist turbulence in simple models of the atmosphere has some precedents. Several years ago, Lapeyre and Held (2004) examined the statistical properties of midlatitude vortices that emerge in moist two-layer turbulence. Their model assumed quasi-geostrophic flow on the beta plane, and applied continual forcing toward baroclinic instability. In sharp contrast, the present investigation examines freely evolving ageostrophic turbulence on the tropical f -plane. Our cumulus parametrization is also distinct.

The remainder of this article is organized as follows. Section 2 formally presents the three-layer model that is used for our investigations. Sections 3–5 describe numerical simulations of hurricane formation in DET. Specifically, section 3 describes the initial conditions and parameter regime of the simulation set. Section 4 surveys the structure of tropical cyclones that emerge in DET under various conditions. Section 5 addresses the time-scale for tropical cyclogenesis, and describes the process by which a tropical depression intensifies into a hurricane in the model. Section 6 summarizes our results and provides some additional discussion on the importance of investigating DET.

2. A simple model for the study of DET

2.1. Basic description

Figure 2 illustrates the idealized troposphere in which we consider the evolution of DET. The model consists of

a boundary layer (0), a middle layer (1) and an upper layer (2). The boundary layer has constant density ρ_0 and fixed thickness H_0 . The middle layer has constant density ρ_1 and variable thickness $h_1(x, y, t)$, in which x , y and t denote the horizontal Cartesian coordinates and time, respectively. The upper layer has constant density ρ_2 and variable thickness $h_2(x, y, t)$. The layer densities are related by

$$\rho_2 = \epsilon\rho_1 \text{ and } \rho_0 = \rho_1, \tag{1}$$

in which ϵ is a positive constant less than unity. The horizontal velocity field of layer $\kappa \in \{0, 1, 2\}$ is independent of the vertical coordinate z and is denoted by $\mathbf{u}_\kappa(x, y, t)$. The underlying ocean supplies moist entropy to the boundary layer and exerts surface friction.

As mentioned earlier, the cumulus parametrization loosely follows that of Ooyama (1969). The O69 paradigm is largely based on the notion that cumulus activity is correlated to convergence of convectively unstable air in the boundary layer, and takes the additional step of *restricting* the development of cumulus updrafts to regions of positive boundary layer convergence.

To elaborate, convergence of boundary layer air generates a mass flux into the middle layer. Subsequently, deep or semi-shallow convection occurs. As defined here, deep convection entrains mass during its rise to the upper troposphere, whereas semi-shallow convection loses mass to the middle layer. Either form of cumulus convection involves a net conversion of dense air to rarefied air, which is analogous to warming of an atmospheric column. Deep convection rarefies more mass than is supplied to the cumulus updraft by the boundary layer, whereas semi-shallow convection rarefies less. The occurrence of deep or semi-shallow convection depends on the value of a local entrainment parameter $\eta(x, y, t)$. The entrainment parameter exceeds unity where the moist entropy of the boundary layer is greater than the saturation entropy of the upper layer. In this case, convergence of boundary

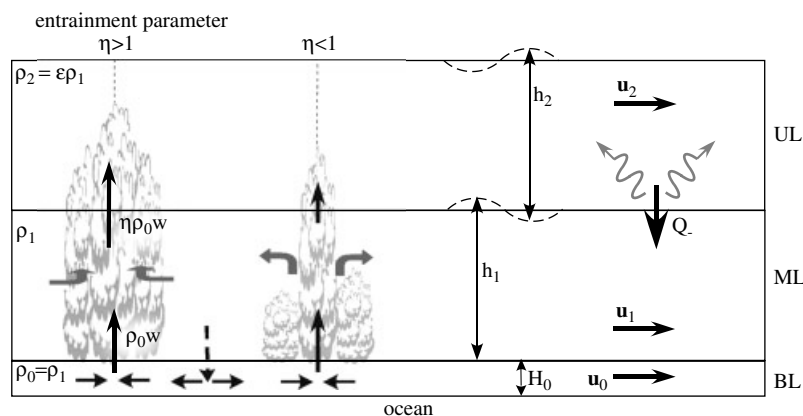


Figure 2. The model troposphere used here to study DET consists of three-layers: a boundary layer (BL), a middle layer (ML) and an upper layer (UL). Convergence of air in the boundary layer stimulates deep (semi-shallow) convection where the entrainment parameter η is greater than (less than) unity. The underlying ocean imposes surface friction and provides a source of moist entropy for the boundary layer that can elevate η above unity. Downdrafts of clear air from the middle layer occur where the boundary-layer flow field diverges. Radiative cooling causes a slow uniform mass transfer from the rarefied upper layer to the middle layer. See section 2 for further details.

layer air generates deep convection. Otherwise, η falls below unity and semi-shallow convection occurs.[‡]

In addition to cumulus updrafts, our model includes two kinds of downdrafts. To begin with, clear air from the middle layer (which has a low value of moist entropy) subsides into regions where the boundary layer flow-field diverges. Furthermore, radiative cooling generates a downward mass flux from the upper layer to the middle layer.

The remainder of section 2 presents details of the dynamical system.

2.2. The mass continuity equations

Because the boundary layer has constant depth, its mass continuity equation reduces to

$$\nabla \cdot \mathbf{u}_0 = -w/H_0. \quad (2)$$

Here, $w(x, y, t)$ is the resolved vertical velocity at $z = H_0$, and $\nabla \equiv \hat{x}\partial_x + \hat{y}\partial_y$ is the horizontal gradient operator. Where w is positive, the magnitude of $\rho_0 w$ corresponds to the outgoing cumulus mass flux. Where w is negative, the magnitude of $\rho_0 w$ corresponds to the incoming mass flux of clear air from the middle layer.

The mass continuity equations of the middle and upper layers are given by

$$\partial_t h_1 + \nabla \cdot (\mathbf{u}_1 h_1) = -Q_+ + \epsilon Q_- + w, \quad (3)$$

and

$$\partial_t h_2 + \nabla \cdot (\mathbf{u}_2 h_2) = Q_+/\epsilon - Q_-, \quad (4)$$

in which Q_+ and Q_- are associated with diabatic mass fluxes. Specifically, the quantity $\rho_1 Q_+$ is the upward mass flux at the interface between the middle and upper layers, due to cumulus convection. The quantity $\rho_2 Q_-$ is the downward mass flux at the same interface, due to radiative cooling.

Following O69, we assume that

$$Q_+ = \eta \frac{\rho_0 w_+}{\rho_1} = \eta w_+, \quad (5)$$

in which

$$w_+ \equiv w \Theta(w). \quad (6)$$

Here, we have introduced the Heaviside step function Θ , which is unity or zero if its argument is positive or negative, respectively. The quantity $\eta - 1$ is the ratio of entrained mass to boundary layer mass in a cumulus updraft. A negative value indicates detrainment in the middle layer. The specific formula for η is a key component of the cumulus parametrization, which is presented in section 2.4.

Radiative cooling acts to counter the vertical expansion/contraction of the upper/middle layer by cumulus

activity. The following basic formula is used for the radiation-driven mass flux:

$$Q_- = \frac{\langle h_2 \rangle - H_2}{\tau_{\text{rad}}}, \quad (7)$$

in which $\langle \dots \rangle$ is the domain average of the quantity in triangular brackets and τ_{rad} is the time-scale at which the system relaxes toward radiative equilibrium, defined by $\langle h_2 \rangle = H_2$.

2.3. The momentum equations

The momentum equation for the boundary layer has the form

$$\begin{aligned} \partial_t \mathbf{u}_0 + \mathbf{u}_0 \cdot \nabla \mathbf{u}_0 = & -\nabla \phi_0 - f \hat{z} \times \mathbf{u}_0 \\ & + \frac{\mathbf{u}_1 - \mathbf{u}_0}{H_0} w_- + \mu \frac{\mathbf{u}_1 - \mathbf{u}_0}{H_0} \\ & - \frac{C_D}{H_0} |\mathbf{u}_0| \mathbf{u}_0 + \frac{1}{H_0} \nabla \cdot \mathbf{S}_0. \end{aligned} \quad (8)$$

The first term on the right-hand side represents forcing by the hydrostatic pressure perturbation, $\rho_0 \phi_0$, which we will shortly relate to h_1 and h_2 . The second term is the usual Coriolis acceleration. The third term represents vertical momentum transport by clear-air subsidence, and introduces the variable

$$w_- \equiv -w \Theta(-w). \quad (9)$$

Note that $w \equiv w_+ - w_-$. The fourth term supposedly represents vertical momentum transport by subgrid eddies and is proportional to the coefficient μ of interface friction. The fifth term accounts for surface friction, and is proportional to the variable drag coefficient $C_D(|\mathbf{u}_0|)$. The last term accounts for lateral eddy viscosity, expressed as the inverse of layer thickness times the divergence of a stress tensor \mathbf{S}_0 .

The momentum equation for the middle layer is given by

$$\begin{aligned} \partial_t \mathbf{u}_1 + \mathbf{u}_1 \cdot \nabla \mathbf{u}_1 = & -\nabla \phi_1 - f \hat{z} \times \mathbf{u}_1 \\ & + \Theta(1 - \eta)(1 - \eta) w_+ \frac{\mathbf{u}_0 - \mathbf{u}_1}{h_1} \\ & + \Theta(Q_-) Q_- \epsilon \frac{\mathbf{u}_2 - \mathbf{u}_1}{h_1} \\ & + \mu \frac{\mathbf{u}_2 + \mathbf{u}_0 - 2\mathbf{u}_1}{h_1} + \frac{1}{h_1} \nabla \cdot \mathbf{S}_1. \end{aligned} \quad (10)$$

As before, the first and second terms on the right-hand side represent the pressure gradient and Coriolis forces. Likewise, the last two terms represent interface friction and lateral eddy viscosity. The middle terms are unique, and account for momentum mixing upon cumulus detrainment and radiation-driven downdrafts.

[‡]Note that semi-shallow convection ($\eta < 1$ in a convergence zone) was not explicitly discussed in O69.

The momentum equation for the upper layer is given by

$$\begin{aligned} & \partial_t \mathbf{u}_2 + \mathbf{u}_2 \cdot \nabla \mathbf{u}_2 \\ &= -\nabla \phi_2 - f \hat{z} \times \mathbf{u}_2 + \Theta(1 - \eta)\eta w_+ \frac{\mathbf{u}_0 - \mathbf{u}_2}{\epsilon h_2} \\ &+ \Theta(\eta - 1)w_+ \frac{\mathbf{u}_0 + (\eta - 1)\mathbf{u}_1 - \eta\mathbf{u}_2}{\epsilon h_2} \\ &- \Theta(-Q_-)Q_- \frac{\mathbf{u}_1 - \mathbf{u}_2}{h_2} + \mu \frac{\mathbf{u}_1 - \mathbf{u}_2}{\epsilon h_2} + \frac{1}{h_2} \nabla \cdot \mathbf{S}_2. \end{aligned} \quad (11)$$

The right-hand side is similar to the forcing of the middle layer, but distinct expressions represent momentum mixing by cumulus convection. The formal difference is readily explained. In the middle layer, cumuli can only deposit mass from the boundary layer. In the upper layer, cumuli can deposit mass from both layers of the lower troposphere if $\eta > 1$.

A complete description of the momentum equations requires precise definitions of several key variables. The definition of ϕ_κ includes an arbitrary constant. For consistency with O69, we let

$$\phi_0 = \phi_1 \equiv g(h_1 - H_1) + \epsilon g(h_2 - H_2), \quad (12)$$

$$\phi_2 \equiv g(h_1 - H_1) + g(h_2 - H_2), \quad (13)$$

in which H_1 and H_2 are the initial ambient values of h_1 and h_2 .

The parametrizations of surface friction and lateral eddy viscosity are subtle issues. For surface friction, we use the following formula of O69:

$$C_D = C_{D*}(1.0 + |\mathbf{u}_0|/u_*), \quad (14)$$

in which C_{D*} is a dimensionless coefficient of order 10^{-3} , and $u_* = 8.33 \text{ m s}^{-1}$. Although Equation (14) is outdated for precise atmospheric modelling (Black *et al.*, 2007), it suffices for the present investigation. For the lateral eddy viscosity, we let

$$\nabla \cdot \mathbf{S} \equiv \sum_{lm} \partial_m [v h (\partial_m u_l + \partial_l u_m)] \hat{x}_l, \quad (15)$$

in which l and m belong to the set $\{0, 1\}$, ∂_m is the partial derivative with respect to the horizontal Cartesian coordinate x_m , and \hat{x}_l is the unit vector parallel to the x_l -axis. The form of \mathbf{S} is the same for all layers, therefore we have suppressed the layer index κ . Notably, our choice of \mathbf{S} belongs to the ‘physical’ class of stress tensors defined by Shchepetkin and O’Brien (1996) (see also Schär and Smith, 1993). For all but one numerical experiment, the kinematic viscosity ν is held constant.

2.4. The η equation

Perhaps the simplest scheme for DET would use a constant value for η : zero would correspond to complete detrainment of boundary layer air into the middle

layer, unity would correspond to zero entrainment of air from the middle layer, and values greater than unity would involve some positive entrainment. The constant- η scheme has some theoretical value, but does not allow the system to self-regulate its convective stability. Instead, we let

$$\eta = \eta_c \equiv 1 + \frac{\theta_{e0} - \theta_{e2}^*}{\theta_{e2}^* - \theta_{e1}}, \quad (16)$$

in which θ_{e0} is the equivalent potential temperature (EPT) of the boundary layer, θ_{e1} is the EPT of the middle layer and θ_{e2}^* is the saturation EPT of the upper layer.

O69 derived the formula $\eta = \eta_c$ under the key assumption that a cloud parcel that is a mixture of air from the bottom two layers must conserve its moist static energy as it ascends into the upper layer, where it becomes neutrally buoyant. His derivation tacitly required that η_c should equal or exceed unity. In order to allow detrainment in the middle layer if $\theta_{e0} < \theta_{e2}^*$, we here extend the applicability of Equation (16) to values of η_c less than unity. We also impose upper and lower limits on η , which are specified in section 3. If η_c exceeds the upper limit η_u , then $\eta = \eta_u$. If η_c is less than the lower limit η_l , then $\eta = \eta_l$.

To complete the parametrization, we need equations for θ_{e0} , θ_{e1} and θ_{e2}^* . The variation of EPT in the boundary layer is determined by the following prognostic equation:

$$\begin{aligned} \partial_t \theta_{e0} + \mathbf{u}_0 \cdot \nabla \theta_{e0} &= w_- \frac{\theta_{e1} - \theta_{e0}}{H_0} \\ &+ C_E |\mathbf{u}_0| \frac{\theta_{es}^* - \theta_{e0}}{H_0} + \nabla \cdot \nu \nabla \theta_{e0}, \end{aligned} \quad (17)$$

which includes negative and positive sources from the middle layer and sea-surface, respectively. The entropy exchange coefficient is given by

$$C_E(|\mathbf{u}_0|) = C_{E*}(1.0 + |\mathbf{u}_0|/u_*) = \frac{C_{E*}}{C_{D*}} C_D. \quad (18)$$

The local saturation EPT at the sea-surface (θ_{es}^*) is assumed to vary linearly with the hydrostatic surface pressure anomaly, $\delta p = \rho_0 \phi_1$. Therefore, we let

$$\theta_{es}^* \equiv \bar{\theta}_{es}^* - \frac{\beta}{c_{pd}} \phi_1, \quad (19)$$

in which $\bar{\theta}_{es}^*$ defines the ambient state, c_{pd} is the specific heat of dry air at constant pressure, and β is a positive constant that is readily estimated (O69).

As in O69, we here use a constant-value approximation for the EPT of the middle layer:

$$\theta_{e1} = \text{constant} < \theta_{e2}^*. \quad (20)$$

Fixing the value of θ_{e1} gives a measure of deep conditional instability, $\theta_{e0} - \theta_{e2}^*$, primary control over convection (Equation (16)). A prognostic equation for θ_{e1} may be used for future studies, in order to investigate the

effects of mid-level moistening on tropical cyclogenesis in DET.

As explained in section 2.1, increasing the value of h_2 [= $H_2 + (\phi_2 - \phi_1)/g(1 - \epsilon)$] corresponds to local warming. Accordingly, the saturation EPT of the upper layer increases with the difference between the upper and lower geopotentials. In a linear approximation, we have

$$\theta_{e2}^* = \bar{\theta}_{e2}^* + \frac{\alpha}{c_{pd}}(\phi_2 - \phi_1), \quad (21)$$

in which $\bar{\theta}_{e2}^*$ is the initial ambient value of θ_{e2}^* and α is another positive constant that is readily estimated (O69).

2.5. Finite-difference approximation and boundary conditions

The spatio-temporal discretization of the model follows standard techniques in atmospheric modelling. The dry, frictionless dynamical core is based on the potential-entropy-conserving finite-difference scheme of Sadourny (1975), which involves computations on four horizontally staggered grids. All EPTs, η and w are defined on the ‘mass’ grid along with h_κ . Functions of η , w and h_κ that are required to evaluate convective momentum transfers are evaluated on the mass grid, and then interpolated on to the horizontal velocity grids. A fourth grid is used for auxiliary computations of vorticity. The flow is moved forward with a time-split algorithm that incorporates an Asselin–Robert filter for numerical stability (Skamarock and Klemp, 1992). For simplicity, the simulation domain is periodic in x and y .

3. Overview of the numerical experiments

3.1. Tropical settings

In general, each simulation involves the evolution of weak turbulence in the lower troposphere toward a dominant convective cyclone. The ‘climate’ parameters and

Table I. Fixed parameters for the primary DET experiments.

Parameters	Values
H_0, H_1, H_2	1 km, 5 km, 5 km
ϵ	0.9
α, β	10.0, 2.0
θ_{e1}	332 K
$\bar{\theta}_{e2}^*$	342 K
η_l, η_u	0, 2.5
τ_{rad}	5 days
μ	$5.0 \times 10^{-4} \text{ m s}^{-1}$
ν	$10^3 \text{ m}^2 \text{ s}^{-1}$
u_*	8.33 m s^{-1}
g	9.8 m s^{-2}
c_{pd}	$1005.7 \text{ J kg}^{-1} \text{ K}^{-1}$

latitude are chosen to resemble tropical conditions. The coefficients of air–sea interaction include realistic values and unrealistic extremes that are of theoretical interest. The simulation domain spans 2000 km in both x and y , and the horizontal grid increment is normally 3.9 km.

Table I lists the specific control parameters that are common to all simulations; they are taken directly from O69. Those related to the initial thermal structure of the free atmosphere are derived from the ambient tropical sounding of Jordan (1958). Table II lists the variable control parameters for multiple simulation sets. The range of the Coriolis parameter f corresponds to latitudes of 5–20°N. The surface-exchange coefficients have typical values of order 10^{-3} (Black *et al.*, 2007). The initial time-scales for momentum and entropy exchange between the ocean and boundary layer are defined by

$$\tau_D \equiv \frac{H_0}{C_D \left(\langle \mathbf{u}_0^2 \rangle^{1/2} \right) \cdot \langle \mathbf{u}_0^2 \rangle^{1/2}}$$

and

$$\tau_E \equiv \frac{C_{D*}}{C_{E*}} \tau_D. \quad (22)$$

Table II. Variable parameters for the primary DET experiments.

Simulation set	RPIs	$\bar{\theta}_{es}^* - \bar{\theta}_{e2}^*$ (°C), T_s (°C)	C_{D*} (10^{-3}), τ_D (days)	$\frac{C_{E*}}{C_{D*}} = \frac{\tau_D}{\tau_E}$	f (10^{-5} s^{-1})
A	1,2	20, 27.7	0.5, 5.7	1	5
B	1,2	25, 28.7	0.5, 5.7	1	5
C	1–4	30, 29.7	0.5, 5.7	1	5
D	1,2	35, 30.7	0.5, 5.7	1	5
E	1	40, 31.6	0.5, 5.7	1	5
F	1,2	30, 29.7	0.25, 11.5	2	5
G	1,2	30, 29.7	1.0, 2.9	0.5	5
H	1,2	30, 29.7	1.5, 1.9	0.33	5
I	1,2	30, 29.7	2.0, 1.4	0.25	5
J	2	30, 29.7	4.0, 0.7	0.125	5
K	1,2	30, 29.7	0.5, 5.7	0.5	5
L	1,2	30, 29.7	0.5, 5.7	1.5	5
M	1,2	30, 29.7	0.5, 5.7	1	2.5
N	1,2	30, 29.7	0.5, 5.7	1	1.25

The values of τ_D and τ_E vary between 0.7 and 11.5 days. The ambient saturation value for the sea-surface EPT ($\bar{\theta}_{es}^*$) varies between 362 and 382 K. The corresponding SSTs (T_s) are derived by inverting the following equation (Emanuel, 1994):

$$\bar{\theta}_{es}^* = T_s \left(\frac{p_s}{p_s - e_{s*}} \right)^{R_d/(c_{pd} + c_l q_{s*})} \exp \left[\frac{L_v q_{s*}}{(c_{pd} + c_l q_{s*}) T_s} \right]. \quad (23)$$

Here, $p_s = 10^5$ Pa is the assumed ambient surface pressure, $e_{s*}(T_s)$ is the ambient vapour pressure of saturated surface air and $q_{s*}(T_s, p_s)$ is the vapour mixing ratio of saturated surface air. In addition, R_d is the gas constant of dry air, c_l is the specific heat of liquid water and $L_v(T_s)$ is the latent heat of vapourization. For our simulations, we find that T_s assumes typical tropical values of 27.7–31.6 °C.

3.2. Initial turbulence

Invariably, the bottom and middle layers start with the same relative vorticity distribution ζ , whereas the upper layer starts at rest. The lower-velocity and height fields are obtained by inverting ζ under the assumption of quasi-balanced flow. Appendix A provides details of the inversion. The approximate balance conditions exclude cumulus convection and minimize inertia–gravity waves. The initialization also sets θ_{e0} equal to θ_{e2}^* , such that η everywhere equals unity.

Each initial vorticity distribution of the lower troposphere is one of several that were randomly generated for this study. In every case, the enstrophy and kinetic energy spectra decay as k^{-1} and k^{-3} , respectively, where k is the horizontal wavenumber of a constituent Fourier mode. The spectra are bounded between wavelengths of 50 and 1000 km; shorter and longer waves have negligible amplitude. The initial conditions differ in the random phases (but not in the amplitudes) of the Fourier modes of ζ . The particular phase configuration is labelled by the random phase index (RPI). A simulation is identified by its set label (A–N), followed by its RPI (1–4).

The initial root-mean-square (rms) of the relative vorticity distribution is $4 \times 10^{-5} \text{ s}^{-1}$. The Rossby number, $Ro \equiv \langle \zeta^2 \rangle^{1/2} f^{-1}$, ranges from 0.8 to 32; consequently, the initial conditions are ageostrophic. The external and internal Froude numbers are defined by

$$Fr^2 \equiv \frac{\langle \mathbf{u}_0^2 \rangle}{g H_T} \quad \text{and} \quad Fr_\sigma^2 \equiv \frac{\langle \mathbf{u}_0^2 \rangle H_T}{\sigma g [H_0(1 - \langle \eta \rangle) + H_1] H_2}, \quad (24)$$

in which $H_T \equiv H_0 + H_1 + H_2$ and $\sigma \equiv 1 - \epsilon$. Given that the initial rms wind speed is 3 m s^{-1} , we have $Fr^2 = 8.3 \times 10^{-5}$ and $Fr_\sigma^2 = 4.0 \times 10^{-3}$ at $t = 0$. Since both initial Froude numbers are much less than unity, the

turbulence is unlikely to generate a significant level of inertia–gravity waves prior to the convective intensification of constituent vortices (Polvani *et al.*, 1994; Ford *et al.*, 2000; Schecter and Montgomery, 2006; Schecter 2008).

Note that the spectral properties and balance conditions of the initial state are not specifically motivated by tropical data; rather, they correspond to the ‘enstrophy range’ of 2D turbulence (Danilov and Gurarie, 2000). Here, we view the initial state merely as a form of garden-variety chaos, with physically plausible wind speeds. Section 5.2 briefly addresses sensitivity to the spectral distribution.

3.3. Generic evolution

Figure 1(b,c) exemplifies the evolution of the initial conditions into a tropical cyclone. With one notable exception, explained below, the parameters of this simulation are equivalent to those of C1. As explained earlier, the initial stage of self-organization resembles ordinary 2D turbulence, in which like-sign vortices coalesce and filaments are chaotically stirred. Convection gradually develops, and the flow skews toward cyclonic dominance. Over time, a distinguished region of cyclonic vorticity engulfs lesser cyclones in the immediate vicinity, and erupts into a dominant hurricane. Section 5.3 illustrates the process of rapid intensification in greater detail.

Figure 1(c) shows the development of cumulus activity, defined quantitatively by

$$CA \equiv w(\eta - 1), \quad w > 0. \quad (25)$$

The variable CA is defined only in regions of boundary-layer convergence. Large positive values indicate massive deep cumuli. Negative values indicate regions of semi-shallow convection, where updrafts partially detrain mass into the middle layer. Apparently, deep convection prevails in cyclones, whereas semi-shallow convection amid subsidence prevails in anticyclones. As in reality, the final hurricane possesses a distinct eye and spiral rainbands. In this figure, the bright/dark half of the grey-scale covers three decades of positive/negative cumulus activity (CA_\pm). All data points with $|CA| < 10^{-3} \max\{|CA|\} \equiv CA^c(t)$ are mapped on to zero.

It is worth noting that the viscosity coefficient in the example under consideration varies with space and time according to $\nu(\mathbf{x}, t) = 0.025(\delta x)^2 |\nabla \cdot \mathbf{u}|$, in which $\delta x = 3.9 \text{ km}$ is the horizontal grid increment. This special parametrization allows lower than normal diffusion/dissipation in areas of weak convergence and convection. Nevertheless, the depicted transformation of DET into a hurricane has no major differences from simulation C1, in which ν is held constant. For simplicity, we use constant viscosity for our primary investigations.

The divergence of DET from ordinary 2D turbulence, as shown here, relates to an obvious fundamental difference between the two dynamical systems. In the absence of external forcing, conservation of energy has an important role in regulating the self-organization of ideal 2D

flows. On the other hand, DET is free to leave its initial energy surface in phase space, and fall into a distinct radiative convective equilibrium (Vallis *et al.*, 1997; Tompkins and Craig, 1998; Robe and Emanuel, 2001; Bretherton *et al.*, 2005; Held *et al.*, 2007; Held and Zhao, 2008). This equilibrium is not constrained by the initial energy, but by a required balance between convective energy input and energy lost by surface drag and radiation.

4. Tropical cyclone structure in DET

4.1. Typical vortex

Before considering the details of tropical cyclogenesis in DET, let us briefly discuss the end state. Figure 3 illustrates the characteristics of a typical equilibrium hurricane. The primary circulation is defined by the azimuthal velocity field v , whereas the secondary circulation is defined by the radial velocity u and the vertical velocity w . As expected for a warm core cyclone, the primary circulation decays with increasing altitude z . Beyond the eye of the storm, v decays with radius r as r^{-q} , in which q is less than unity owing to an outer skirt of cyclonic vorticity. The secondary circulation is characterized by boundary-layer inflow, outflow aloft and a distinct eye-wall updraft near the radius of maximum wind.

The thermal structure of the DET hurricane is partially consistent with that of a real tropical cyclone. The radial distribution of θ_{e2}^* properly reflects a warm core, and θ_{e0} properly decays with increasing r beyond the radius of maximum wind. At the periphery of the storm, which is not shown in the figure, the boundary layer EPT is 352 K. On the other hand, θ_{e0} is unrealistically low in the eye. [This result is at odds with observations (Montgomery *et al.*, 2006), full-physics simulations (Zhang *et al.*, 2002) and the axisymmetric, balanced, three-layer hurricane simulations of O69.] The moist entropy hole is artificially caused by pockets of subsidence that force θ_{e0} toward θ_{e1} , which has no warm-core correction to its ambient value. Despite its unphysical appearance, the moist entropy hole is not entirely unwelcome in the context of our model, since it keeps the eye free of deep convective instabilities.

Another notable feature of the steady state is the overall expansion of the upper layer at the expense of the middle layer. This reflects the fact that the radiative convective equilibrium involves a warmer atmosphere than the pure radiative equilibrium, in which $\langle h_2 \rangle = H_2$.

4.2. Parameter dependence of vortex intensity

Figure 4 shows the variation of tropical cyclone intensity with the following control parameters:

$$\bar{\theta}_{es}^* - \bar{\theta}_{e2}^*, \quad C_{D*}, \quad C_{E*} \quad \text{and} \quad f.$$

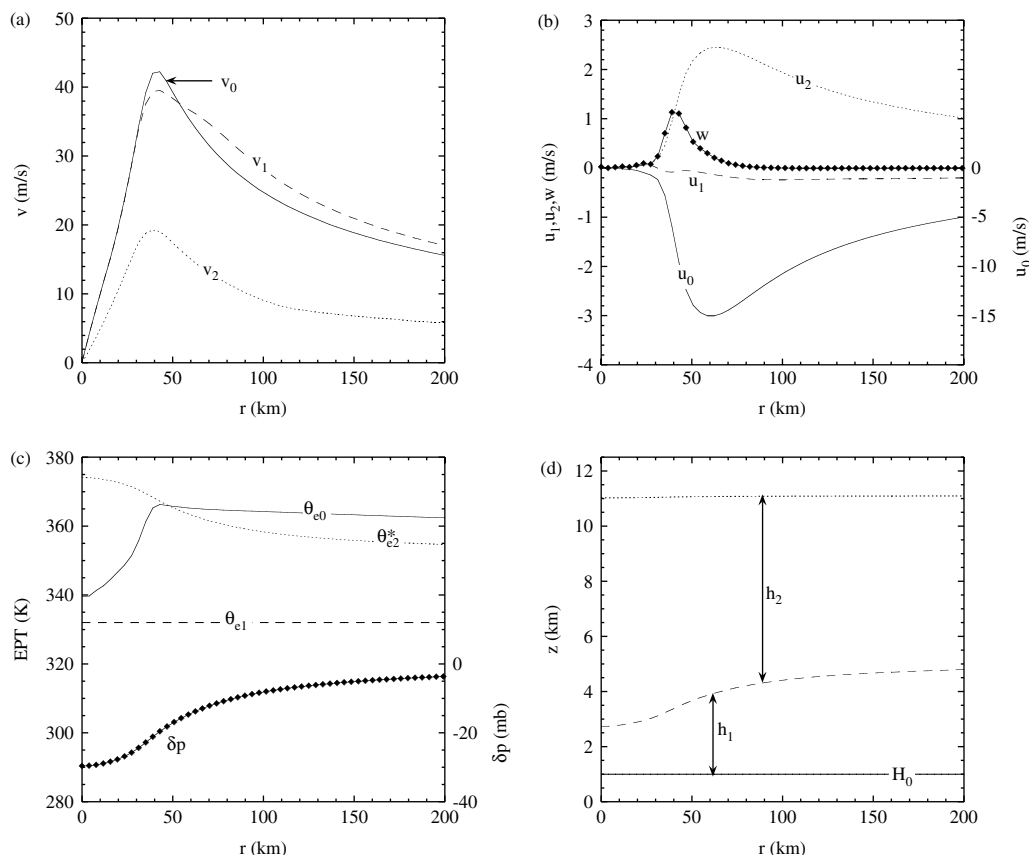


Figure 3. Typical DET hurricane. (a) Tangential velocities. (b) Radial velocities and vertical velocity at the top of the boundary layer. (c) Equivalent potential temperatures and surface pressure anomaly. The numerical value of δp is calculated under the assumption that $\rho_0 = 1 \text{ kg m}^{-3}$. (d) Layer heights. The data are from simulation C1 at 3.9 km resolution; all fields are azimuthal means, averaged over the time-interval $36.63 \leq t \leq 38.33$ days.

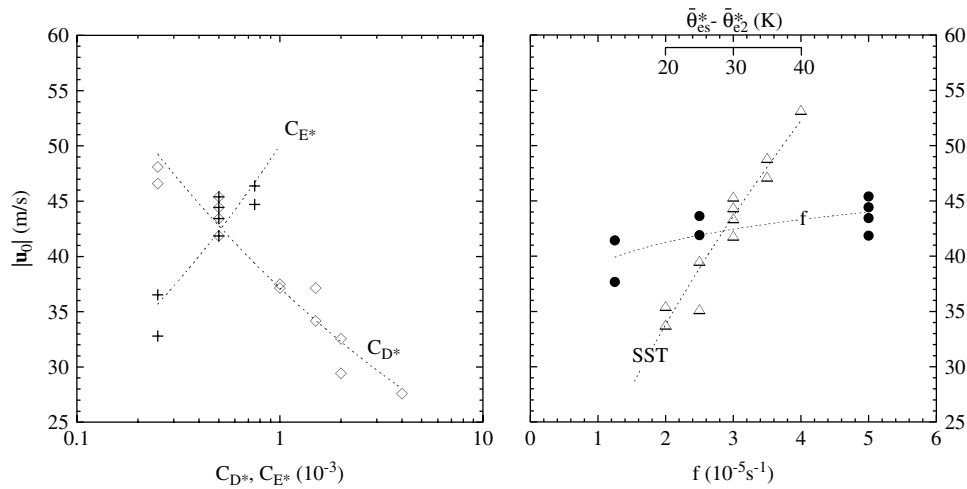


Figure 4. Maximum boundary layer wind speed of tropical cyclones in simulations A–N, versus several control parameters. The triangles represent simulation sets A–E, which vary only in the SST. The diamonds represent simulation sets C and F–J, which vary only in C_{D*} . The crosses represent simulation sets C and K–L, which vary only in C_{E*} . The circles represent simulation sets C and M–N, which vary only in f . The plotted data are from simulations with 3.9 km resolution. Furthermore, the wind speeds are temporal averages over many minor fluctuations. Each dashed curve shows the basic trend of the maximum wind speed with variation of the indicated control parameter.

The first parameter is viewed as a measure of the SST. The middle two parameters control the impact of surface friction and surface entropy exchange, whereas the Coriolis parameter indicates the level of ambient rotation at a given latitude. The variation of each parameter is carried out keeping all others fixed. Each variation intersects the point in parameter space that defines simulation set C. The numerical experiments are qualitatively consistent with current tropical cyclone theory (Emanuel 1986, 1995b). The vortex amplifies with increasing SST or C_{E*} , but weakens with increasing C_{D*} .[§] Furthermore, the intensity varies only slightly with latitude between 5°N and 20°N.

It is worth noting that the maximum intensity of a DET hurricane in gradient balance is limited by the condition that the central ($r = 0$) value of h_1 remain positive. At sufficiently high values of the SST or of the ratio C_{E*}/C_{D*} , the hurricane intensifies to the unphysical regime where gradient balance requires negative h_1 . This ‘hypercanes’ catastrophe coincides with numerical instability.

4.3. Parameter dependence of vortex size

Tropical cyclones are known to show a broad range of spatial scales under similar ambient conditions. As the following demonstrates, such is not the case in our numerical experiments. Greater diversity might occur with a larger domain, a lower eddy viscosity or a different initial energy spectrum. However, there are no obvious reasons why such experimental modifications should radically change the variation of mean vortex size (radius of maximum wind) with climate and air–sea interaction parameters.

[§]Recent cloud-resolving numerical simulations (Nolan *et al.*, 2007) have shown that tropical cyclone intensity varies less dramatically with the SST when the ambient sounding of the atmosphere is initialized to that of radiative-convective equilibrium in a small domain.

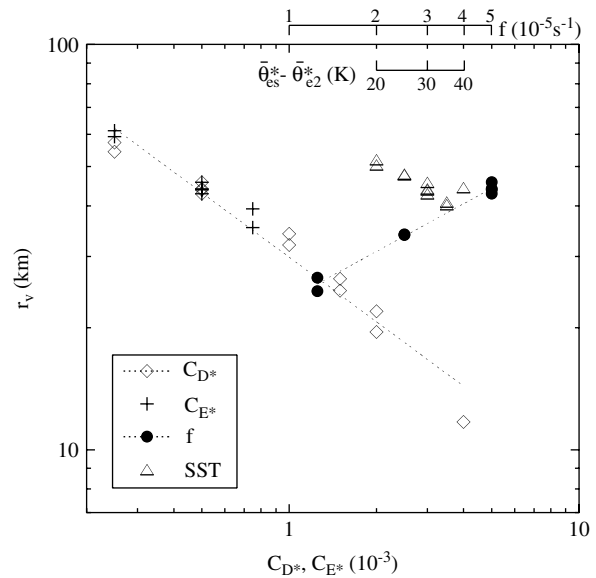


Figure 5. Radius of maximum tangential wind speed *versus* several control parameters. The data set and symbols are the same as in Figure 4.

Figure 5 shows the radius of maximum tangential wind speed r_v under various conditions. The steady-state cyclone contracts with increasing values of the SST, C_{E*} or C_{D*} . However, the cyclone widens with increasing values of f . A simulation on the equator ($f = 0$) produced a weak tropical storm after several months of ‘gestation’. We have excluded this data point from the figure, because r_v was too small for us to assume adequate resolution.

In contrast to our result, Held and Zhao (2008) found that the mean vortex radius decreases with greater ambient rotation in GCM-like simulations on the periodic f -plane. The discrepancy may stem from their larger domains, or their relatively large grid increments,

which could not have resolved our equilibrium vortices. Conflicting results of this kind motivate future investigations on the sensitivity of steady-state scaling laws to different parametrizations of cumulus convection and air-sea interaction.

4.4. Fluctuations

Needless to say, the steady-state hurricane that develops from DET is not a true equilibrium. Rather, it exhibits irregular intensity oscillations that are connected to the instability, decay and regeneration of its eyewall. The peak-to-trough variation of the maximum boundary layer wind speed during an eyewall cycle is of order 10 m s^{-1} in the strongest hurricanes considered: the data in Figures 3–5 are temporal averages over one or many fluctuations. Since viscosity and diffusivity affect eyewall instability and the fine-scale features of convection, details of the eyewall cycle vary with their representations. Sensitivity to horizontal resolution is also an issue. In order to limit the scope of this article, a thorough analysis of eyewall cycles in our model is deferred to a future publication.

5. Tropical cyclogenesis in DET

5.1. Atmospheric stability

Some understanding of atmospheric stability in our model is necessary for discussing tropical cyclogenesis. As in complimentary models of similar complexity, our cumulus parametrization has a nonlinear influence on small perturbations (Crum and Dunkerton, 1992, 1993; Frierson *et al.*, 2004; Khouider and Majda, 2007). Nonlinearity deeply complicates stability analysis. For the present discussion, let it suffice to consider an analogous system that has a linear parametrization of diabatic processes (cf. O69).

In the analogous linear system, the *total* diabatic mass flux at the interface between the middle and upper layers is given by

$$\rho_0(Q_+ - \epsilon Q_-) = \rho_0 \eta w,$$

in which η is constant. Using a constant value for η is tantamount to assuming that any perturbation to the basic thermal structure of the atmosphere is negligible. Unconditional proportionality between the diabatic mass flux and w implies that boundary layer divergence is connected to local cooling of the free atmosphere in the same way that convergence is connected to local warming. For the time being, let us also neglect surface drag, lateral eddy viscosity and interface friction.

A small perturbation about the rest state can be viewed as a superposition of plane waves proportional to $e^{i(kx - \omega t)}$, in which k is the wavenumber and x is the Cartesian coordinate in the direction of propagation. The dispersion relation is obtained by substituting a plane wave solution into the continuity and momentum

equations, and neglecting terms that are second-order in the wave amplitude. The result is given below:

$$\omega^2(\omega^2 - f^2) \left\{ (\omega^2 - f^2)^2 - (\omega^2 - f^2)gH_T k^2 - g^2 \sigma H_2 [H_0(\eta - 1) - H_1] k^4 \right\} = 0. \quad (26)$$

For any given wavevector, there are eight independent solutions: two geostrophically balanced modes, two barotropic inertia-gravity waves, two baroclinic inertia-gravity waves and two convective inertial modes.

The geostrophic modes are stationary, and the inertial modes are characterized by $\omega = \pm f$. Assuming that $\sigma \equiv 1 - \epsilon \ll 1$, the dispersion relation for the barotropic inertia-gravity waves reduces to

$$\omega^2 = f^2 + gH_T k^2. \quad (27)$$

Moreover, the dispersion relation for the baroclinic inertia-gravity waves reduces to

$$\omega^2 = f^2 + \sigma g \frac{[H_0(1 - \eta) + H_1]H_2}{H_T} k^2. \quad (28)$$

The baroclinic inertia-gravity waves are stable ($\omega^2 > 0$) at any value of f or k , provided that $\eta < 1 + H_1/H_0$. This condition is enforced in all of our numerical simulations. Otherwise, deep convection could suffer an ultraviolet catastrophe, in which the modal growth rate diverges as the magnitude of k tends toward infinity.

So, under ordinary circumstances, finite surface friction is required for instability. Our numerical model is complicated by the fact that surface friction is quadratic to lowest order in the velocity field. For simplicity, we may consider an alternative linear parametrization, in which

$$C_D |\mathbf{u}_0| \rightarrow \hat{C}_D = \text{constant}.$$

Linear surface drag changes the growth rate (the imaginary part of ω) of a geostrophic mode from zero to the following:[¶]

$$\Im[\omega] = \frac{\hat{C}_D}{H_1} \frac{\eta - 1 - (H_1/H_2)\xi^2}{1 + (H_1 + H_2)\xi^2/H_2 + (H_1/H_2)\sigma\xi^4}, \quad (29)$$

in which

$$\xi^2 \equiv \frac{f^2}{\sigma g H_1 k^2} \equiv \frac{\lambda^2}{8\pi^2 l_R^2}, \quad (30)$$

$\lambda = 2\pi/k$ is the horizontal wavelength and $l_R \equiv \sqrt{\sigma g H_1 / 2f^2}$ is the internal Rossby length. A similar expression is found in O69. A formal derivation requires that $\omega/f \ll \hat{C}_D / (fH_0) \ll 1$ and $H_0 \ll H_1, H_2$. The geostrophic mode is stable at scales greater than l_R , for the usual situation in which H_1 is of order H_2 , and η

[¶]Surface friction may also destabilize fast convective modes, such as the baroclinic inertia-gravity waves.

is of order unity. At small scales, the mode grows only if η exceeds unity. This condition permits the cooperative intensification (CI) of deep cumulus convection and the horizontal winds, stimulated by Ekman pumping. The intensification rate is proportional to the surface drag coefficient.

It is unreasonable to assume that linear CI directly applies to the amplification of finite-amplitude perturbations in a model with nonlinear parametrizations of cumulus convection and air–sea interaction (O69; Ooyama, 1982). The inadequacy of linear theory is obvious, since our simulations of tropical cyclogenesis initially satisfy a sufficient condition for linear stability ($\eta = 1$). On the other hand, setting C_{D*} equal to zero prevents tropical cyclogenesis, as predicted by linear CI. Furthermore, instability occurs after wind-induced surface entropy fluxes have time to increase the value of η above unity (DeMaria and Pickle, 1988; Dengler and Reeder, 1997). Therefore it seems likely that a form of quasi-linear CI governs tropical cyclogenesis in the model.

5.2. Primary genesis time-scale

Let us now return to the numerical results. Figure 6 shows the time τ_{10} at which the maximum wind speed in the boundary layer reaches 10 m s^{-1} under various conditions. By this time, a distinguished tropical depression clearly begins convective intensification toward a tropical storm or hurricane. First note that τ_{10} decreases with increasing values of C_{D*} , C_{E*} and the SST. Such behaviour is not surprising in view of quasi-linear CI, in which the instantaneous amplification rate of the disturbance increases with C_{D*} and η . Clearly, increasing the surface exchange coefficient for moist entropy accelerates the growth of η ; the same is true of raising the SST (see Equation (17)).

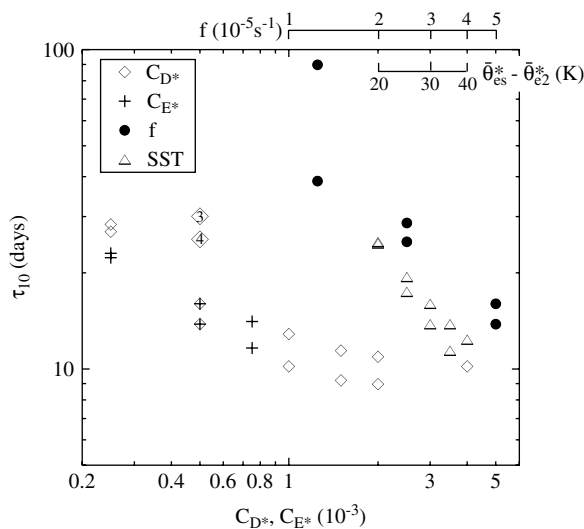


Figure 6. The time τ_{10} required for a dominant tropical depression to form and reach a maximum wind speed of 10 m s^{-1} , versus several control parameters. The data set and symbols are the same as in Figure 4. Unlike previous figures, only the scatter-plot for variation of C_{D*} includes points from simulations C3 and C4. The corresponding diamonds are clearly labelled.

The variation of τ_{10} with latitude is perhaps a more subtle issue. Here, we observe that the initial stage of tropical cyclogenesis accelerates (τ_{10} decreases) at higher latitudes. Linear CI predicts the opposite behaviour, but also assumes quasi-geostrophic motion. Quasi-geostrophic scaling is clearly invalid, since the Rossby number of the initial turbulence is of order unity or greater. Slower development at lower latitudes is more consistent with the rare occurrence of real tropical cyclogenesis near the equator. It is also sensible that a lower reservoir of planetary vorticity would inhibit the formation of hurricanes.

Despite fairly robust trends, the genesis time τ_{10} may vary significantly with the random phase index (RPI) of the initial turbulence for a given set of control parameters. Due to practical limitations at relatively high resolution, the simulation sets considered here are generally too small to reveal substantial variability. Simulation sets C and N are exceptions. In set C, which includes four ‘observations’, the standard deviation of τ_{10} is 36% of the mean, which is roughly one week.

Changing the power spectrum of the initial conditions reveals a more profound level of stochastic behaviour. The following demonstration involves two simulations that are similar to those of set M. In both cases, the long-wave cut-off of the initial turbulence is reduced to 400 km, and the rms wind speed of the lower troposphere is reduced to 2.4 m s^{-1} . The two initial conditions differ only in the random phases of the constituent Fourier modes. Figure 7 illustrates the evolution of both simulations. One flow evolves into a tropical cyclone, whereas the other relaxes to a synoptic scale circulation. Evidently, subtle changes to the initial conditions can prevent the development of tropical cyclones from turbulence. Such nonlinear bifurcation underscores the limitations of purely linear thinking.

For further insight, we briefly examined the intensification of isolated low-level cyclones, with radial length-scales of 200–300 km at $t = 0$. The control parameters were identical to those of set C. The initial conditions satisfied gradient balance with no secondary circulation. The rms and maximum wind speeds were 2.5 m s^{-1} and $7.2\text{--}5.4 \text{ m s}^{-1}$, respectively. For additional consistency with the turbulence simulations, we set η everywhere equal to unity. The time required for the maximum wind speed of the cyclone to pass 50 m s^{-1} was 20–35% of the mean τ_{10} of set C. Not surprisingly, an isolated cyclone develops into a mature hurricane substantially faster than a ‘similar’ turbulent flow field is able to create an incipient tropical depression.

5.3. Rapid, asymmetric intensification

Following the development of a tropical depression in DET, the vortex rapidly intensifies to its steady state. Figure 8 illustrates the corresponding evolution of relative vorticity in the middle layer. Initially, the vorticity distribution amplifies in a thin ring where the cyclonic winds are peaked. A shear-flow instability then breaks the ring into multiple mesovortices (Schubert *et al.*, 1999).

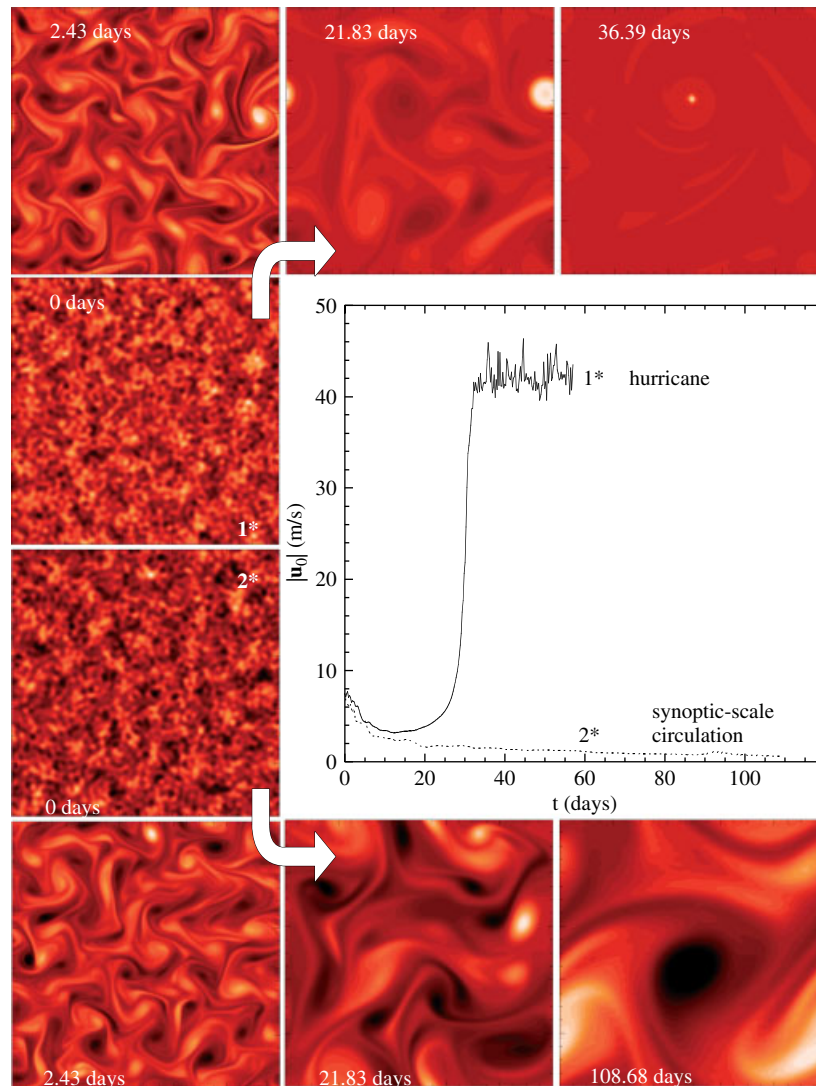


Figure 7. Two potential paths of DET with spectrally equivalent initial conditions. The colour contour plots, which span 2000 km in both horizontal dimensions, show the evolution of relative vorticity in the middle layer. The colour scale readjusts instantaneously, as in Figure 1. The enclosed graph shows the evolution of the maximum boundary layer wind speed. The initial turbulence transforms into either a hurricane or a synoptic-scale circulation. Note: the parameters of the simulations shown here are identical to those of set M, but the initial turbulence is confined to smaller scales, as explained in the text.

The mesovortices exhibit chaotic motion superposed on contraction of the entire system. Ultimately, the flow transforms into a more symmetric, quasi-stationary hurricane.

Figure 9 shows the variation of the intensification rate γ with three of the primary control parameters of the model. The intensification rate is defined by the following equation:

$$\gamma \equiv \ln \left(\frac{\langle |\mathbf{u}_0| \rangle_{\tau_*}^+}{\langle |\mathbf{u}_0| \rangle_{\tau_{10}}^+} \right) \frac{1}{\tau_* - \tau_{10}}. \quad (31)$$

Here, $\langle \dots \rangle^+$ is the w_+ -weighted average of the quantity in triangular brackets, over the entire domain of the simulation. The weight factor w_+ is nonzero (and positive) only where cumulus convection exists; moreover, it increases with the cumulus mass flux into the middle layer. Under such weighting, the eyewall of the dominant storm contributes most to the average. The subscript '10'

or '*' indicates that the average is evaluated at time τ_{10} or τ_* , respectively. The value of τ_* is the time at which $\langle |\mathbf{u}_0| \rangle^+$ reaches 80% of its maximum. The intensification rate γ increases with the SST and the surface exchange coefficient for moist entropy, as does the formation rate of a tropical depression. In contrast, γ slightly decays with increasing latitude.

The variation of γ with surface friction deserves more detailed discussion, due to the controversial nature of the subject. Axisymmetric, cloud-resolving numerical simulations have shown that increasing the surface drag coefficient slightly reduces the intensification rate (Craig and Gray, 1996; Gray and Craig, 1998). Here, γ increases sharply with surface friction until C_{D*} passes 10^{-3} , at which point its growth is more gradual (Figure 10(a)). Resolving the continual growth of γ with increasing surface friction requires increasingly fine resolution. Presumably, finer grids are necessary because higher surface friction reduces the scale of the tropical cyclone in our model

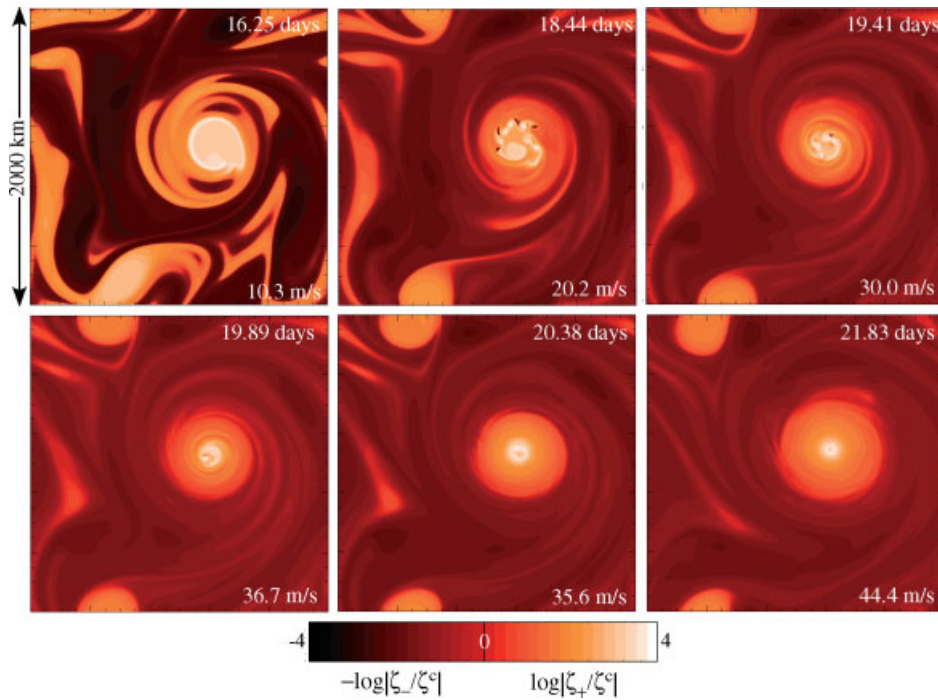


Figure 8. The evolution of relative vorticity ζ in the middle layer during the asymmetric intensification of a tropical depression into a hurricane. The data are from simulation C1, at 2 km resolution. The printed velocities are the instantaneous maximum wind speeds in the middle layer. The bright/dark half of the logarithmic colour scale covers four decades of positive/negative vorticity (ζ_{\pm}). All data points with $|\zeta| < 10^{-4} \max\{|\zeta|\} \equiv \zeta^c(t)$ are mapped on to zero.

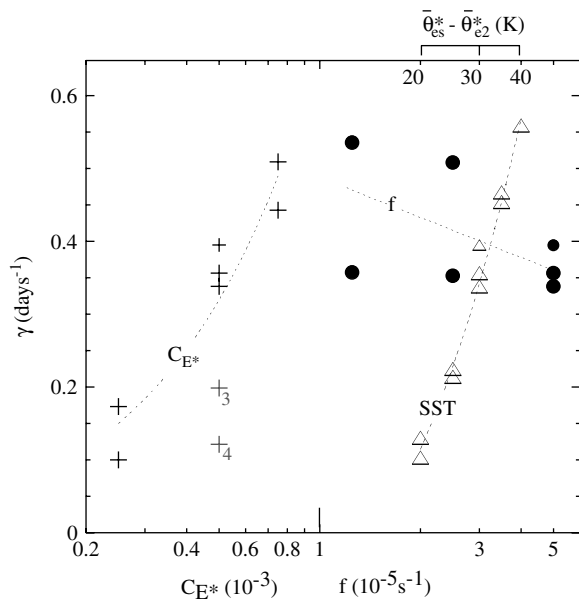


Figure 9. The measured intensification rate γ of a tropical depression into a hurricane versus several control parameters. The relationship between the symbol shape and the varied parameter is the same as in Figure 4. The smaller symbols correspond to simulation C1, with the horizontal grid increment reduced from 3.9 to 2 km prior to intensification. Only the scatter-plot for variation of C_{E^*} includes points from simulations C3 and C4, as indicated.

(Figure 5). Lowering the resolution to 7.8 km actually reverses the trend of γ over a broad interval of C_{D^*} .

Although the intensification of a tropical depression into a tropical storm or hurricane appears to be a strongly nonlinear process, it is tempting to test the quantitative

relevance of quasi-linear thinking. Let us first define a quasi-linear CI parameter by the following:

$$\gamma_c(t) \equiv \left\langle \frac{C_D(|\mathbf{u}_0|) \cdot |\mathbf{u}_0| (\eta - 1)}{h_1} \right\rangle^+ \quad (32)$$

In the regime of our simulations, where $\xi^2 \ll 1$, γ_c amounts to the average growth rate of linear CI in areas of cumulus convection (Equation (29)). Figure 11 plots γ_c versus time for a typical simulation (C1). The time series of the domain maximum of $|\mathbf{u}_0|$ is superposed on the graph,^{||} along with the time series for the w_+ -weighted averages of θ_{e0} and θ_{e2}^* . Clearly, amplification of wind speed corresponds to positive γ_c . Moreover, the sudden saturation of maximum wind speed coincides with an abrupt transition of γ_c to a negative value. Following this transition, the average deep conditional instability $\langle \theta_{e0} - \theta_{e2}^* \rangle^+$ fluctuates near zero.

It is natural to hypothesize that the vortex intensification rate γ is proportional to the CI parameter. Could this agree with the observed nonlinear scaling of γ with the surface drag coefficient? The preceding question is answered affirmatively by comparing γ with the time-averaged CI parameter,

$$\bar{\gamma}_c \equiv \frac{1}{\tau_* - \tau_{10}} \int_{\tau_{10}}^{\tau_*} \gamma_c dt \quad (33)$$

Figure 10(b) demonstrates that

$$\gamma = a \bar{\gamma}_c \quad (34)$$

^{||}The time series of $\langle |\mathbf{u}_0| \rangle^+$ follows a similar trend, but exhibits slow decay after rapid intensification.

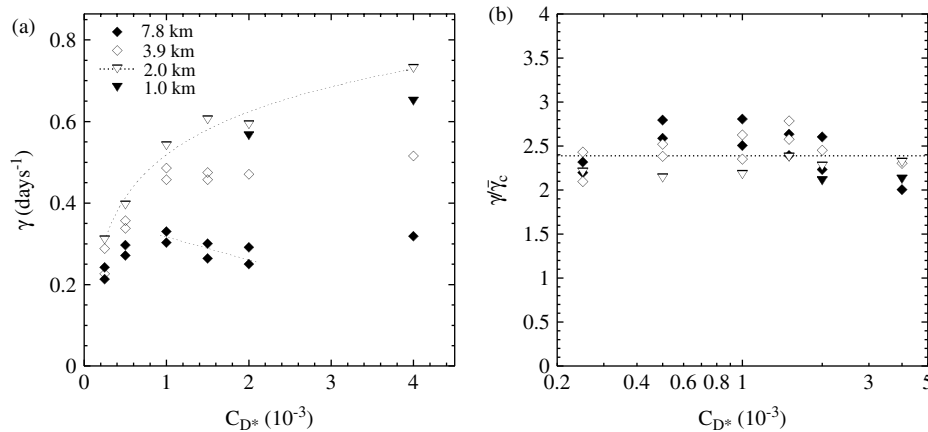


Figure 10. The influence of surface friction on rapid intensification. (a) The intensification rate γ versus C_{D*} for simulation sets C and F–J (with RPIs of 1 and 2) at four different resolutions, both higher and lower than normal. Severe slowdown and a trend reversal occur at the lowest (7.8 km) resolution. (b) The intensification rates in (a) normalized to the time-averaged CI parameter $\bar{\gamma}_c$.

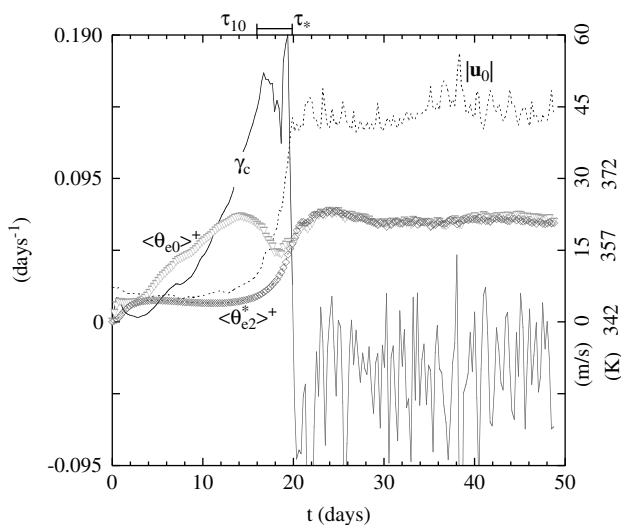


Figure 11. Time series of the CI parameter (Equation (32)) in simulation C1, at 3.9 km resolution. Superposed on this graph are time series for the maximum boundary-layer wind speed, the boundary layer EPT and the saturation EPT of the upper layer. The bar at the top of the graph shows the time-averaging interval for γ and $\bar{\gamma}_c$.

in which $a = 2.4 \pm 0.4$ for all intensification events at all resolutions, in a simulation set (C, F–J) where C_{D*} varies over a wide range of values. Result (34) is especially interesting, because it holds at coarse resolution, where secondary structures are poorly resolved, and the derivative of γ with respect to C_{D*} is negative over a large interval.

Before concluding, let us briefly address the issue of quasi-equilibrium vortex development. It has been proposed that tropical cyclones gradually intensify from one state of approximate equilibrium to another (Emanuel, 1995a; Gray and Craig, 1998). The equilibrium of a convective vortex (in our model) is characterized in part by the approximate equivalence of θ_{e0} and θ_{e2}^* in convectively active regions. Conceivably, intensification via quasi-equilibrium could occur. However, Figure 11 illustrates a more typical scenario in which $\langle \theta_{e0} \rangle^+$ is substantially greater than $\langle \theta_{e2}^* \rangle^+$ as a tropical depression transforms into a hurricane.

6. Summary and conclusion

Until recently, the theoretical study of hurricane formation has focused on the evolution of an isolated cyclone. Hurricane formation in DET is a more general paradigm, in which incipient storms are exposed to a variety of positive and negative interactions with neighbouring vortical structures. This article examined the time required for tropical cyclogenesis in DET, and the structure of steady-state vortices. For simplicity, we used a three-layer model of the troposphere with an O69-like cumulus parametrization. The primary purpose of this first article was to introduce the subject of DET, not to examine every possible variant. Future investigations with alternative models and more realistic initial conditions are planned.

As expected for a process that is fuelled by the moist entropy supply of the underlying ocean, we found that tropical cyclogenesis in DET accelerates with increasing values of the SST and C_{E*} . Increasing the Coriolis parameter accelerates the formation of an incipient tropical cyclone, but slightly hinders the subsequent stage of rapid intensification. Increasing the value of C_{D*} tends to shorten both stages of genesis. This result is sensible for O69-like models, in which Ekman pumping plays a critical role in stimulating cumulus convection. After rapid intensification, the positive feedback of surface friction becomes negative, in the sense that increasing C_{D*} reduces the equilibrium vortex intensity.

In agreement with state-of-the-art cloud-resolving numerical simulations (Nguyen *et al.*, 2008), we have also shown that cyclone intensification is a complex, asymmetric process. In our model, intensification involves a shear-flow instability, followed by the production of mesovortices and radial contraction of the basic circulation. Accurate simulation of intensification requires that the secondary structures in the developing storm are resolved. Inadequate resolution was shown to severely reduce the intensification rate γ and negate its derivative with respect to the surface drag coefficient. Although the transformation of a tropical depression into a hurricane is highly nonlinear, we found that averaging the

rate of linear CI (Equation (32)) over the area of substantial cumulus convection, and over the period of rapid intensification, correctly gives the order of magnitude of γ . Moreover, the vortex intensity saturates when the (weighted) spatial average of the linear CI rate abruptly drops toward zero, due to local warming of the upper troposphere.

Whereas the evolution of an isolated cyclone is deterministic in simple models, the formation of hurricanes in DET is clearly less predictable. This point is underscored by the existence of bifurcation phenomena, in which spectrally equivalent manifestations of turbulence can develop into either a hurricane or a synoptic-scale circulation. Further examination of the local conditions (near an incipient storm) that are required to allow hurricane formation in DET may improve our understanding of what permits the actual event in nature. Conceivably, knowledge gained from such investigations could improve the statistical forecasting of tropical cyclogenesis (McBride and Zehr, 1981; DeMaria *et al.*, 2001, 2005).

Although we have focused on simulations that produce a single tropical cyclone, it is worth noting that the attractors of DET (the statistically stationary end-states) can have much richer characteristics. We have begun to examine late-time solutions in larger domains, where multiple hurricanes may coexist amid occasional mergers (Held and Zhao, 2008). These more complex states reveal the potential importance of convective filaments in the background flow. We have observed that filaments provide seeds for the generation of new convective vortices. Furthermore, filaments entrained by hurricanes can form outer convective rings, which replace inner eye-walls. Continued investigation of how the characteristics of DET in larger domains vary with climate and air-sea interaction parameters may prove to be a fruitful endeavour.

Acknowledgements

The authors thank Professors Isaac Held and Roger Smith and the editors of this journal for constructive reviews of this manuscript. This work was funded by the National Science Foundation of the United States of America, through grant ATM-0750660. The numerical results were partly obtained using supercomputers at the National Center for Atmospheric Research, Boulder, CO.

Appendix A: ‘Balanced’ initial conditions

By design, the initial conditions of the numerical simulations satisfy

$$\nabla \cdot \mathbf{u}_\kappa = 0, \quad (\text{A1})$$

in which κ is the layer index. Zero divergence implies that the velocity field is the cross-gradient of a streamfunction, that is

$$\mathbf{u}_\kappa = \hat{\mathbf{z}} \times \nabla \psi_\kappa. \quad (\text{A2})$$

In general, a vorticity field ζ_κ is specified and the streamfunction is obtained by inverting the Poisson equation,

$$\nabla^2 \psi_\kappa = \zeta_\kappa. \quad (\text{A3})$$

Furthermore, the initial conditions are supposed to satisfy

$$\partial_t \nabla \cdot \mathbf{u}_\kappa = 0. \quad (\text{A4})$$

Our implementation of Equation (A4) is inexact, because it neglects surface friction ($C_D = 0$), interface friction ($\mu = 0$) and eddy viscosity ($\nu = 0$). As such, it becomes

$$\left. \begin{aligned} \psi_0 &= \psi_1, \\ \nabla^2 h_1 &= \frac{B_1 - \epsilon B_2}{g\sigma}, \\ \nabla^2 h_2 &= \frac{B_2 - B_1}{g\sigma}, \end{aligned} \right\} \quad (\text{A5})$$

in which

$$B_\kappa \equiv f \zeta_\kappa + 2(\partial_{xx} \psi_\kappa)(\partial_{yy} \psi_\kappa) - 2(\partial_{xy} \psi_\kappa)^2. \quad (\text{A6})$$

The top line of (A5) states that the boundary layer and the middle layer have identical flows. The bottom lines simplify to the following, under the operational assumption that the upper layer is initially at rest ($\psi_2 = 0$):

$$\nabla^2 h'_1 = B_1/g\sigma, \quad h'_2 = -h'_1, \quad (\text{A7})$$

in which $h'_\kappa \equiv h_\kappa - H_\kappa$ and $\langle h'_\kappa \rangle$ is set equal to zero.

References

- Arakawa A. 2004. The cumulus parametrization problem: past, present and future. *J. Climate* **17**: 2494–2525.
- Black PG, D’Asaro EA, French JR, Drennan WM, Niller PP, Sanford TB, Terrill EJ, Walsh ED, Zhang JA. 2007. Air–sea exchange in hurricanes: Synthesis of observations from the coupled boundary layer air–sea transfer experiment. *Bull. Am. Meteorol. Soc.* **88**: 357–374.
- Boffetta G, Celani A, Vergassola M. 2000. Inverse energy cascade in two-dimensional turbulence: Deviations from Gaussian behavior. *Phys. Rev. E* **61**: R29–R32.
- Bretherton CS, Blossy PN, Khairoutdinov M. 2005. An energy-balance analysis of deep convective self-aggregation above uniform SST. *J. Atmos. Sci.* **62**: 4273–4292.
- Celani A, Cencini M, Mazzino A, Vergassola M. 2004. Active and passive fields face to face. *New J. Phys.* **6**: paper 72:1–35.
- Craig GC, Gray SL. 1996. CISK or WISHE as the mechanism for tropical cyclone intensification. *J. Atmos. Sci.* **53**: 3528–3540.
- Crum FX, Dunkerton TJ. 1992. Analytic and numerical models of wave-CISK with conditional heating. *J. Atmos. Sci.* **49**: 1693–1708.
- Crum FX, Dunkerton TJ. 1993. CISK and evaporation-wind feedback with conditional heating on an equatorial beta-plane. *J. Meteorol. Soc. Jpn* **72**: 11–18.
- Danilov SD, Gurarie D. 2000. Quasi two-dimensional turbulence. *Physics-Uspekki* **43**: 863–900.
- Danilov SD, Gurarie D. 2001. Nonuniversal features of forced two-dimensional turbulence in the energy range. *Phys. Rev. E* **63**: paper 020203: 1–4.
- DeMaria M, Pickle JD. 1988. A simplified system of equations for simulating tropical cyclones. *J. Atmos. Sci.* **45**: 1542–1554.

- DeMaria M, Schubert WH. 1984. Experiments with a spectral tropical cyclone model. *J. Atmos. Sci.* **41**: 901–924.
- DeMaria M, Knaff JA, Connell BH. 2001. A tropical cyclone genesis parameter for the tropical Atlantic. *Weather and Forecasting* **16**: 219–233.
- DeMaria M, Mainelli M, Shay LK, Knaff JA, Kaplan J. 2005. Further improvement to the Statistical Hurricane Intensity Prediction Scheme (SHIPS). *Weather and Forecasting* **20**: 531–543.
- Dengler K, Reeder MJ. 1997. The effects of convection and baroclinicity on the motion of tropical cyclone-like vortices. *Q. J. R. Meteorol. Soc.* **123**: 699–725.
- Emanuel KA. 1986. An air sea interaction theory for tropical cyclones. Part I: Steady state maintenance. *J. Atmos. Sci.* **43**: 585–604.
- Emanuel KA. 1989. The finite amplitude nature of tropical cyclogenesis. *J. Atmos. Sci.* **46**: 3431–3456.
- Emanuel KA. 1994. *Atmospheric Convection*. Oxford University Press: New York, 580.
- Emanuel KA. 1995a. The behavior of a simple hurricane model using a convective scheme based on subcloud-layer entropy equilibrium. *J. Atmos. Sci.* **52**: 3960–3968.
- Emanuel KA. 1995b. Sensitivity of tropical cyclones to surface exchange coefficients and a revised steady state model incorporating eye dynamics. *J. Atmos. Sci.* **52**: 3969–3976.
- Ford R, McIntyre ME, Norton WA. 2000. Balance and the slow quasi-manifold: some explicit results. *J. Atmos. Sci.* **57**: 1236–1254.
- Frierson DMW, Majda AJ, Paulis OM. 2004. Large scale dynamics of precipitation fronts in the tropical atmosphere: a novel relaxation limit. *Comm. Math. Sci.* **2**: 591–626.
- Gill AE. 1982. *Atmosphere–Ocean Dynamics*. Academic Press: San Diego 662.
- Gray SL, Craig GC. 1998. A simple theoretical model for the intensification of tropical cyclones and polar lows. *Q. J. R. Meteorol. Soc.* **124**: 919–947.
- Held IM, Zhao M. 2008. Horizontally homogeneous radiative–convective equilibria at GCM resolution. *J. Atmos. Sci.* **65**: 2003–2013.
- Held IM, Zhao M, Wyman B. 2007. Dynamic radiative–convective equilibria using GCM column physics. *J. Atmos. Phys.* **64**: 228–238.
- Holton JR. 1992. *An introduction to dynamic meteorology*. Academic Press: San Diego 511.
- Jordan CL. 1958. Mean soundings for the West Indies area. *J. Meteor.* **15**: 91–97.
- Khouider B, Majda AJ. 2007. A simple multicloud parametrization for convectively coupled tropical waves. Part II: Nonlinear simulations. *J. Atmos. Sci.* **64**: 381–400.
- Lapeyre G, Held IM. 2004. The role of moisture in the dynamics and energetics of turbulent baroclinic eddies. *J. Atmos. Sci.* **61**: 1693–1710.
- McBride JL, Zehr RM. 1981. Observational analysis of tropical cyclone formation. Part II: Comparison of nondeveloping versus developing systems. *J. Atmos. Sci.* **38**: 1132–1151.
- Montgomery MT, Bell MM, Abernethy SD, Black M. 2006. Hurricane Isabel (2003). New insights into the physics of intense storms. Part I: Mean vortex structure and maximum intensity estimates. *Bull. Am. Meteorol. Soc.* **87**: 1335–1347.
- Nam K, Ott E, Antonsen TM, Jr, Guzdar P. 2000. Lagrangian chaos and the effect of drag on the enstrophy cascade in two-dimensional turbulence. *Phys. Rev. Lett.* **84**: 5134–5137.
- Nguyen VS, Smith RK, Montgomery MT. 2008. Tropical cyclone intensification and predictability in three dimensions. *Q. J. R. Meteorol. Soc.* **134**: 563–582.
- Nolan DS, Rappin ED, Emanuel KA. 2007. Tropical cyclogenesis sensitivity to environmental parameters in radiative–convective equilibrium. *Q. J. R. Meteorol. Soc.* **133**: 2085–2107.
- Ooyama K. 1969. Numerical simulation of the life cycle of tropical cyclones. *J. Atmos. Sci.* **26**: 3–40.
- Ooyama K. 1982. Conceptual evolution of theory and modelling of the tropical cyclone. *J. Meteorol. Soc. Jpn* **60**: 369–379.
- Pedlosky J. 1987. *Geophysical Fluid Dynamics*. Springer-Verlag: New York 710.
- Polvani LM, McWilliams JC, Spall MA, Ford R. 1994. The coherent structures of shallow-water turbulence: Deformation-radius effects, cyclone/anticyclone asymmetry and gravity-wave generation. *Chaos* **4**: 177–186.
- Raymond DJ. 1995. Regulation of moist convection over the west Pacific warm pool. *J. Atmos. Sci.* **52**: 3945–3959.
- Raymond DJ. 1997. Boundary layer quasi-equilibrium (BLQ). In *The Physics of Parameterization of Moist Convection*, Smith RK (ed). Kluwer Academic: Dordrecht 387–397.
- Robe FR, Emanuel KA. 2001. The effect of vertical wind shear on radiative–convective equilibrium. *J. Atmos. Sci.* **58**: 1427–1445.
- Rotunno R, Emanuel KA. 1987. An air–sea interaction theory for tropical cyclones: Part II. Evolutionary study using a nonhydrostatic axisymmetric numerical model. *J. Atmos. Sci.* **44**: 542–561.
- Sadoury R. 1975. The dynamics of finite-difference models of the shallow-water equations. *J. Atmos. Sci.* **32**: 680–689.
- Schär C, Smith R. 1993. Shallow water flow past isolated topography. Part I: Vortex production and wake. *J. Atmos. Sci.* **50**: 1373–1401.
- Schecter DA. 2008. The spontaneous imbalance of an atmospheric vortex at high Rossby number. *J. Atmos. Sci.* **65**: 2498–2521.
- Schecter DA, Montgomery MT. 2006. Conditions that inhibit the spontaneous radiation of spiral inertia–gravity waves from an intense mesoscale cyclone. *J. Atmos. Sci.* **63**: 435–456.
- Schubert WH, Montgomery MT, Taft RK, Guinn TA, Fulton SR, Kossin JP, Edwards JP. 1999. Polygonal eyewalls, asymmetric eye contraction, and potential vorticity mixing in hurricanes. *J. Atmos. Sci.* **56**: 1197–1223.
- Shapiro LJ. 1992. Hurricane vortex motion and evolution in a three-layer model. *J. Atmos. Sci.* **49**: 140–153.
- Shapiro LJ. 2000. Potential vorticity asymmetries and tropical cyclone evolution in a moist three-layer model. *J. Atmos. Sci.* **57**: 3645–3662.
- Shchepetkin AF, O'Brien JJ. 1996. A physically consistent formulation of lateral friction in shallow-water equation ocean models. *Mon. Weather Rev.* **124**: 1285–1300.
- Skamarock WC, Klemp JB. 1992. The stability of time-split numerical methods for the hydrostatic and the nonhydrostatic elastic equations. *Mon. Weather Rev.* **120**: 2109–2127.
- Smith RK. 2000. The role of cumulus convection in hurricanes and its representation in hurricane models. *Rev. Geophys.* **38**: 465–489.
- Tompkins AM, Craig GC. 1998. Radiative convective equilibrium in a three-dimensional cloud-ensemble model. *Q. J. R. Meteorol. Soc.* **124**: 2073–2097.
- Vallis GK, Shutts GJ, Gray MEB. 1997. Balanced mesoscale motion and stratified turbulence forced by convection. *Q. J. R. Meteorol. Soc.* **123**: 1621–1652.
- Zhang DL, Liu Y, Yau MK. 2002. A multiscale numerical study of Hurricane Andrew (1992). Part V: Inner-core thermodynamics. *Mon. Weather Rev.* **130**: 2745–2763.
- Zehnder JA. 2001. A comparison of convergence- and surface-flux-based convective parametrizations with applications to tropical cyclogenesis. *J. Atmos. Sci.* **58**: 283–301.
- Zhu H, Smith RK. 2002. The importance of three physical processes in a minimal three-dimensional tropical cyclone model. *J. Atmos. Sci.* **59**: 1825–1840.
- Zhu H, Smith RK, Ulrich W. 2001. A minimal three-dimensional tropical cyclone model. *J. Atmos. Sci.* **58**: 1924–1925.